Nanoparticle size and surface chemistry effects on mechanical and physical properties of nano-reinforced polymers: The case of PVDF-Fe3O4 nano-composites

Francisco Sebastian Navarro Oliva, Mehdi Sahihi, Luc Lenglet, Alejandro Ospina, Erwann Guenin, Andres Jaramillo-Botero, William Goddard, Fahmi Bedoui

Nanoparticle size and surface chemistry effects on mechanical and physical properties of nano-reinforced polymers: the case of PVDF-Fe3O4 nano-composites

Francisco Sebastian Navarro Oliva[1], Mehdi Sahihi[1,5], Luc Lenglet[2], Alejandro Ospina[1], Erwann Guenin[3], Andres Jaramillo-Botero[4], William A. Goddard III[4], Fahmi Bedoui[1,4,*]

[1]Roberval Laboratory, Université de Technologie de Compiègne, Alliance Sorbonne Université, Compiègne 60200, France

[2] NORMAFIN, Levallois-Perret, France

[3]TIMR (Integrated Transformations of Renewable Matter) Université de Technologie de Compiègne, France

[4]Materials and Process Simulation Center, California Institute of Technology, Pasadena, California 91125, United States

[5]Université Clermont Auvergne, Clermont Auvergne INP, CNRS, Institut de Chimie de Clermont-Ferrand, F-63000 Clermont-Ferrand, France

*Corresponding author: fahmi.bedoui@utc.fr

ABSTRACT

In the present work, PVDF - Fe_3O_4 nanoparticle (NP) nanocomposite films were produced using the electrospinning method. We investigated the effect of NP size on the film's morphology (fiber size), mechanical properties, and physical properties (β-phase percentage). Surprisingly, while nanoparticle size acts as an enhancer for mechanical properties, it appeared to act as an inhibitor in terms of its effects on the crystallization of the β-polymorph. This result seemed in discordance with many previous results. A focus on local interactions between the NP surface chemistry and PVDF chains revealed the influence of grafted ligands at the nanoparticle surface on the crystallization of the piezoelectric phase of PVDF. The results from the molecular dynamics (MD) simulations for systems of PVDF chains with slabs of -OH and oleic acid-grafted magnetite, showed that the probability of beta phase configuration decreases when the nanoparticles are functionalized with oleic acid and becomes more probable for -OH terminated magnetite. These computational results are in accordance with our experimental results. To

verify this hypothesis, we prepared films with washed nanoparticles to eliminate the excess oleic acid that acts as a β-polymorph inhibitor. As a result, the amount of β-phase obtained for washed nanoparticles increased and the difference in the amount of β-phase between the different samples decreased. Moreover, when heated, the films of nanocomposite with washed NP developed more β-phase for smaller sizes of nanoparticles. At 140 °C, isomerization occurred, and oleic acid was converted into elaidic acid, reducing the steric hindrance, and promoting the interaction between PVDF chains and the surface of the nanoparticles. This isomerization reaction seems to be an enhancer of the α- to β-phase transition. Our results prove that optimizing multiple properties in nano-reinforced polymers requires consideration of different aspects, such as NP size, surface chemistry, and processing methods.

Our results based on mixed experimental and modeling approach proved the usefulness of simulation in understanding and guiding our experimental results. Our results suggest that for enhancing piezoelectric properties in PVDF magnetite nano-composites, the chemistry and the molecular morphology of the grafted ligands when combined with NP size could lead to multi-properties enhancement simultaneously.

Keywords: Size effects, Surface chemistry, Polymer nanocomposites, Poly(vinylidene fluoride), Magnetite, MD Simulation

1 INTRODUCTION

Poly(vinylidene fluoride) (PVDF) has attracted a great deal of attention since the discovery of its piezo-, pyro- and ferroelectricity [1-6]. This thermoplastic fluoropolymer is lightweight, chemically inert, and exhibits several useful properties such as flexibility, resistance to solvents, high purity, biocompatibility, and stability under high electric fields. Thanks to its properties, PVDF can be utilized for several advanced applications including energy harvesters, the design of sensors and actuators, data storage, and drug delivery in medicine, among others [7-11].

PVDF is a semicrystalline polymer that has complex polymorphisms. The three main crystalline phases in PVDF are α, β and γ [9]. The α-phase is non-polar, and its molecular conformation is trans-gauche (TG^+TG^-). The dipole moments of the single molecules cancel each other out in the monoclinic lattice which explains the non-polarity of the α-phase. On the other hand, the β-phase structure is polar, and its molecular conformation is all-trans (TTTT). The dipole moments of the β-phase chains have the same direction, which amplifies the dipole moment in the lattice and confers the piezo- and ferroelectric properties [12]. The γ-phase is also polar, but its molecular conformation is $TTTG^+TTTG^-$. The piezoelectric effect in this structure is weaker than the β-phase because of a gauche bond in every fourth repeat unit [9].

The α-phase is the most common as it is the most thermodynamically stable form of PVDF [9]. However, PVDF phases can be changed by thermal, mechanical, or electric treatments [13-16] e.g., inducing the β-phase by mechanical stretching of the α-phase.

There are different ways of causing the formation of the β-phase, such as mechanical stretching [13, 17], electrospinning [4, 5, 18-20], high electric field polling of α-phase films, and the addition of nanofillers [7, 21, 22].

Preparing PVDF nanocomposites via electrospinning to obtain β-PVDF has attracted attention lately. This manufacturing technique makes use of an electric field to produce nanometric fibers from a polymer solution droplet. External electric fields induce mechanical stretching of the PVDF chains. During the electrospinning process, the chains are stretched by uniaxial forces, which can force the transition to the all-trans conformation of β-PVDF [18-20, 23].

It has been demonstrated that incorporating fillers such as CNTs, nanoclay, nano silicates, some metal oxides nanoparticles, and Ni-Zn ferrite nanoparticles, among others, can cause the formation of β-PVDF.

Incorporating iron oxide (Fe_3O_4) nanoparticles promotes the formation of β-phase PVDF [24, 25]. In PVDF, these effects are attributed to the interaction between the Fe_3O_4 nanoparticle and the -CH_2- groups in PVDF. The -CH_2- groups have a positive charged density and promote the TTTT conformation, inducing the nucleation of β-PVDF [26, 27]. However, the exact mechanism and influence of Fe_3O_4 nanoparticles on the conformational arrangement of PVDF molecules remains unknown. The combined effect of incorporating Fe_3O_4 magnetic nanoparticles and enhancing β-PVDF will help with the development of new electroactive-based materials, such as Néel effect-based sensors [28], exhibiting multiferroic properties.

As the interaction between the PVDF chains and the Fe_3O_4 nanoparticle occurs at the surface of the nanoparticle, its surface chemistry is a factor that must be considered. Although there are many reports about PVDF-Fe_3O_4 nanocomposites, the relationship between PVDF crystallization and the surface chemistry of Fe_3O_4 are less explored. Fe_3O_4 nanoparticles are often functionalized with organic molecules such as oleic acid to promote good dispersion and avoid the formation of aggregates [29-31].

In this work, we aim to study experimentally the influence of the surface chemistry of iron oxide nanoparticles on the crystallization of PVDF in electrospun nanocomposites. Simulated molecular dynamics (MD) effectuated on functionalized models of oleic acid and -OH terminated magnetite slabs and α-PVDF [6] will help first explain our data, then tailor our experimental approach.

2 EXPERIMENTAL

2.1 Electrospinning PVDF-Fe_3O_4 nanocomposite films and PVDF-Oleic acid films

We prepared two mixtures of 1.7 g of PVDF (ref: FV306300, Goodfellow, Ltd, Cambridge, UK) and 200 mg of Fe_3O_4 nanoparticle powder (ref: Ferrotec) (with oleic acid as a surface ligand) with 7 nm and 20 nm respectively in 10 mL of a dimethylformamide (DMF) – acetone mixture (40/60 V/V). The targeted mass fraction of Fe_3O_4 in PVDF was 10% w/w after solvent evaporation during the electrospinning process.

The same protocol was followed to prepare two other mixtures of PVDF and Fe_3O_4 nanoparticles (but the nanoparticles were previously washed with ethanol and toluene to remove the excess oleic acid at their surface [31]). Two PVDF/oleic acid solutions with concentrations of 2% m/m and 4% m/m of oleic acid and a blank test solution of PVDF were also prepared.

Each mixture was stirred at 70°C for 1h (400 rpm), sonicated at 70°C for 1h and loaded into a 5 mL syringe after cooling down for about 20 minutes at room temperature. An automatic KDS-100 pump (KD Scientific) was used to set the flow rate of the mixture to 0.020 mL/min. The conductive collector was placed at 18 cm from the tip of the needle. A voltage of 17.5 kV was imposed between the collector and the needle throughout the 30 minutes of the electrospinning process.

2.1.1 Nanoparticles washing

Fe_3O_4 nanoparticles were washed with ethanol. The suspensions of NPs-ethanol were agitated in an ultrasonic bath for 20 min. The NPs were separated from the washing solvent using a centrifuge machine and a magnet. The NPs were then washed with toluene in the same way.

2.2 Thermogravimetric analysis (TGA)

Thermogravimetric analysis was performed on nanocomposite samples to determine the nanoparticle mass fraction. TGA from SETARAM Instrumentation was utilized to perform tests from 40°C to 1000°C with a heating rate of 15°C/min under an air atmosphere.

2.3 Scanning electron microscopy

Samples were cut into squares (approximately 5×5 mm^2) out of the electrospun film, mounted on carbon discs, metal-coated with gold (5 nm) and observed using a Quanta FEG250 from FEI Environmental Scanning Electron Microscope (SEM). The fiber size distribution was measured manually using the software ImageJ on the SEM images acquired.

2.4 Transmission electron microscopy

The size distribution of Fe_3O_4 NP was determined with a 2100F (JEOL, Ltd) Transmission Electron Microscope (TEM) by applying an acceleration voltage of 200 kV. Carbon-coated mesh grids were used to collect the samples to be analyzed: for the pure Fe_3O_4 NP, a single drop of a suspension of the NPs in toluene was placed on the grid, leaving the solvent to evaporate at room temperature. The NP diameter distributions were quantified manually from

the TEM images acquired using ImageJ (by National Institutes of Health) on at least 200 measures per sample. To obtain the images of the fibers produced by electrospinning, the grid was placed on the collector to allow fibers to deposit for 15s.

2.5 Mechanical characterization – tensile measurements

Tensile tests were performed twice for electrospun films of pure PVDF, PVDF-7 nm Fe_3O_4, and PVDF-20 nm Fe_3O_4 nanocomposites with a testing machine with a 300 N capacity load cell. Samples were cut from the films produced using a pattern 4 mm wide and 15 mm long. The width and thickness of the specimen cut were obtained after cutting with a micrometer and placed in the testing machine, leaving 10 mm between the clamps. The measurements were made at 1.0 mm/min and the force and time were recorded at a rate of 500 ms. The stress and strain were calculated according to equations (1) and (2), as follows:

$$\sigma = \frac{F}{A} \tag{1}$$

$$\varepsilon = \frac{\Delta l}{l_0} \tag{2}$$

where F is the force, A the transversal area of the sample, ΔL the displacement and l_0 the initial gauge length between the clamps. The stress-strain curves of electrospun films were recorded at room temperature, conscious of the qualitative aspect of the testing approach, the data obtained will be used to compare qualitatively the response of the different materials and not to derive mechanical parameters quantitatively.

2.6 X-Ray diffraction (XRD)

To determine the amount of β-phase in each film, room temperature wide angle X-ray scattering (WAXS) studies were performed using a Bruker D8 Advance X-ray diffractometer with an X-ray wavelength of 0.1542 nm, operated at 30 kV and 40 mA. The scanning covered the 2θ range of 10°–30° with increments of 0.02°.

The PVDF-Fe_3O_4 films were analyzed before and after a heat treatment at 140°C for 17 h.

2.7 MD simulation

Initially, we constructed a 79.1×64.5×8.8 $Å^3$ magnetite slab and an α-PVDF layer according to the procedure described in our previous work [6]. The surface of the magnetite slab was treated by replacing the single bonded oxygen (O) atoms with OH groups. Then, 20% of the OH groups were replaced with oleic acid groups. The chemical structures of water and oleic acid were optimized at the level of B3LYP/6–31g** using Gaussian 16 quantum chemistry software (USA) [32], before modification of the magnetite surface.

The α-PVDF layer was placed on top of the magnetite slab and their distance was set to about 5.0 Å. MD simulation calculations were carried out using the simulation package GROMACS version 5.0.7 [33, 34]. The details of the 10 ns MD simulation procedure and force field parameters of all the components are presented in the supporting information (SI-1).

2.8 Fourier transformed infrared spectroscopy (FTIR)

Infrared spectra of a sample of oleic acid before and after thermal treatment at 140°C for 17 hours were obtained *via* a Thermo Scientific Nicolet iS5 Infrared Spectrometer in the range of 400-1500 cm^{-1}, in ATR (attenuated total reflection) mode.

3 RESULTS AND DISCUSSION

The main objective of this work is the investigation of NPs and the effect of their surface chemistry on the morphological, mechanical, and physical properties of the nanocomposites.

3.1 Thermogravimetric analysis (TGA)

We performed TGA tests on the different nanocomposites to examine the mass fraction of the nanoparticles. The curves of PVDF - 7 nm Fe_3O_4 and PVDF - 20 nm Fe_3O_4 were normalized and are shown in **Figure 1**. We observed the weight loss after the heating cycle, in which the polymeric matrix was burned, and the remaining mass allowed us to calculate the mass fraction of the sample. The values obtained were close to 10% w/w, which validated the targeted mass fraction for our samples (10.10 ± 0.08 % for PVDF - 7 nm Fe_3O_4 and 10.51 ± 0.09 % for PVDF - 20 nm Fe_3O_4).

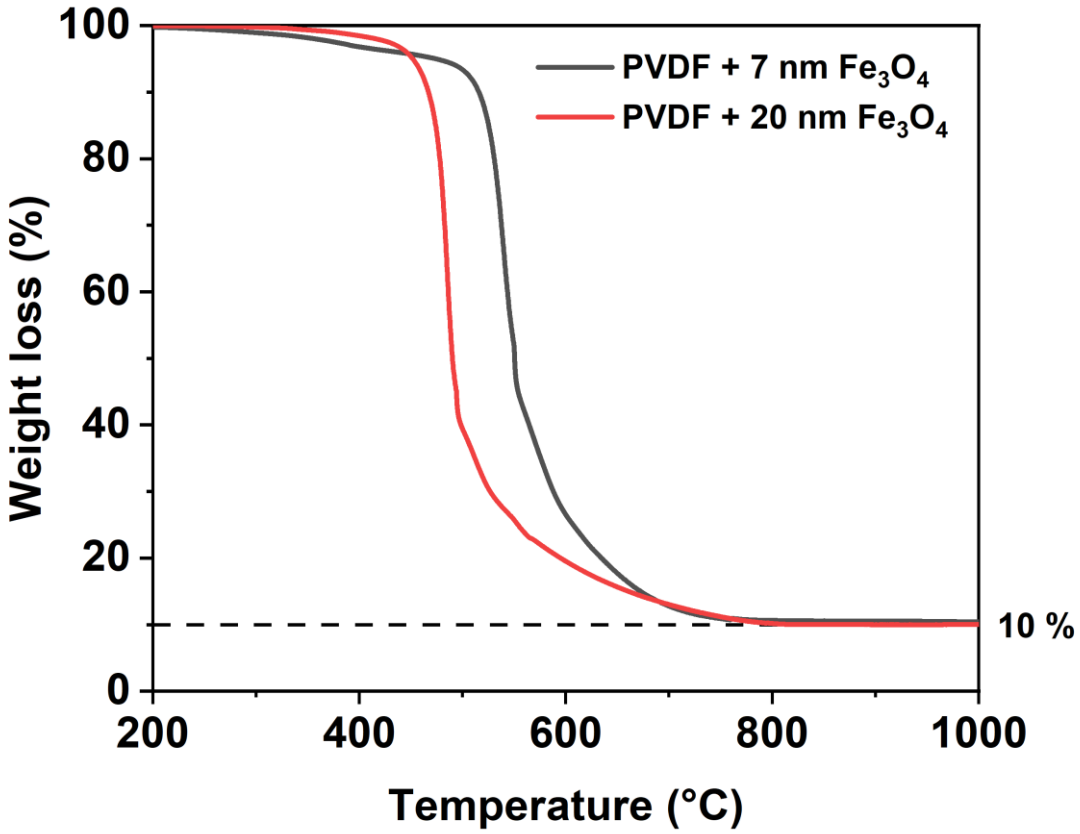

Figure 1 TG curves of PVDF - 7 nm Fe3O4 and PVDF - 20 nm Fe3O4

3.2 Nanoparticle size distribution

TEM images and size distribution of 7 nm and 20 nm Fe_3O_4 nanoparticles are shown in **Figure 2**. They revealed good dispersion thanks to oleic acid functionalization of their surfaces. We noticed that the 20 nm NPs purchased presented a size distribution of around 15 nm ± 1.55 nm and the 7 nm NPs presented a distribution close to their theoretical one (7.09 m ± 0.51 nm).

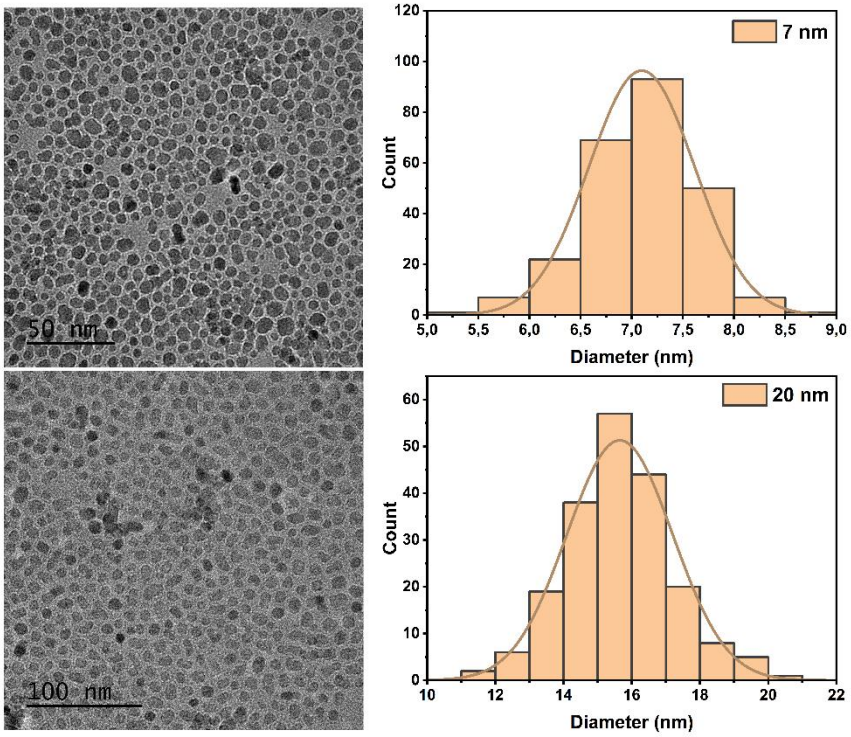

Figure 2 TEM images of (**A**) 7 nm Fe_3O_4 and (**B**) 20 nm Fe_3O_4 nanoparticles

3.3 Fiber size distribution and morphology

The electrospinning process makes it possible to obtain films made of entangled fibers. We investigated the size distribution of the fibers for each electrospun nanocomposite film. We observed an apparent decrease in the fiber distribution of nanocomposites compared to pure PVDF as shown in **Figure 3** SEM images of electrospun nanocomposites and their corresponding fiber size distributions. Moreover, the smaller the nanoparticles, the more this decrease intensifies. These results are in accordance with previous results [35].

We assume this is unequivocally related to the increase in surface-to-volume ratio.

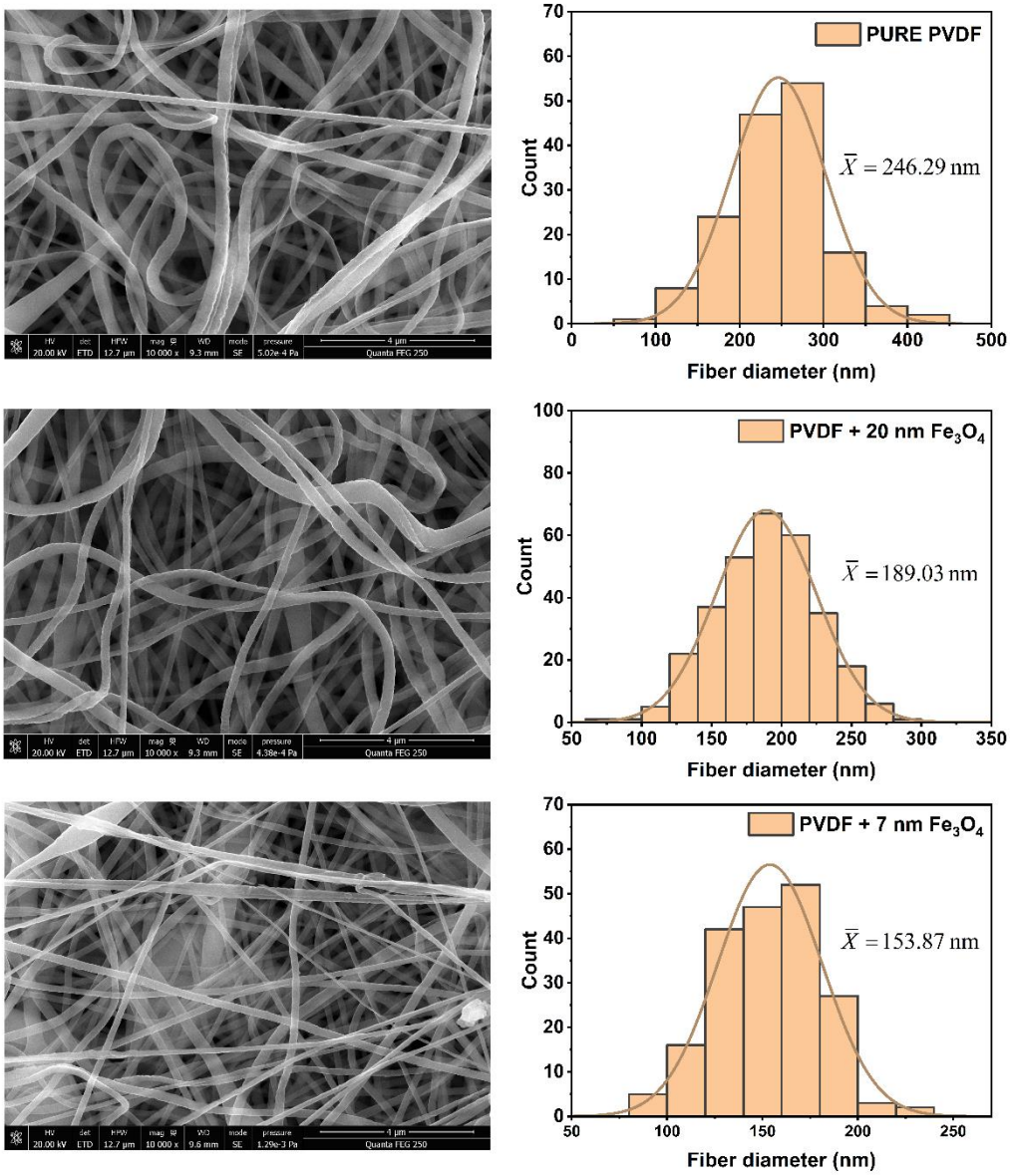

Figure 3 SEM images of electrospun nanocomposites and their corresponding fiber size distributions.

Moreover, Fe_3O_4 nanoparticles are conductive, and the number of conductive nanoparticles is higher for smaller sizes, if we consider constant volume fractions. In this case, the stretching force is stronger. It is therefore possible to deduce that the stretching ratio is higher. This explains a decrease in fiber size for smaller reinforced nanocomposites.

The electrospun fibers in the films are non-aligned. The parameters of electrospinning, the viscosity and concentration of the solution were chosen in order to avoid bead formation [35]. **Figure 4** shows electrospun fibers on TEM carbon-coated grids, with nanoparticles inside, and their diameter distributions.

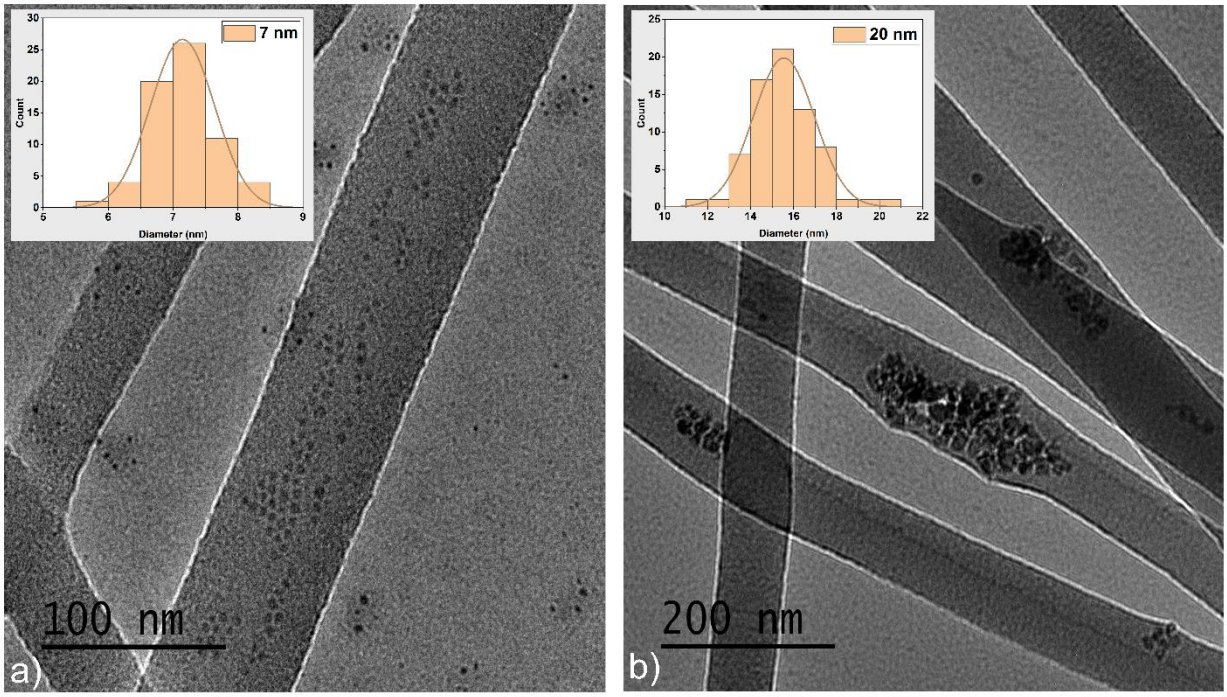

Figure 4 TEM images of PVDF - 7 nm Fe_3O_4 and PVDF - 20 nm Fe_3O_4 electrospun fibers

3.4 Mechanical characterization – tensile measurements

Mechanical testing of an individual electrospun fiber is expected to be the most direct method for studying its mechanical behavior. However, electrospun fibers are usually collected in a non-woven film. Therefore, it was not possible in our case to mechanically characterize single fibers. We characterized the mechanical properties of nanofibrous films based on tensile testing using a universal testing machine (DEBEN MICROTEST system). The tension test

depends on nanofiber diameters, alignment, and the effects of fiber entanglements inside nanofiber films.

Here, the effect of the size of nano-reinforcements on fiber diameter explains the increase in tensile strength of the films with a smaller fiber diameter, as shown in **Figure 5**. The tensile strength of PVDF - 7 nm Fe_3O_4 electrospun films is related to the extended surface-to-volume ratio of their fibers [22, 36]. This translates into an increase in the number of contacts between fibers, which intensifies their entanglement [37, 38]. The physical figure that we can derive in this case is that smaller NPs increase the drawing ratio leading to thinner nanofibers. By decreasing fiber size, we enhance molecular orientation within the fiber and increase fiber entanglement. It is also worth noticing that NPs favor strong interactions at the interface [39].

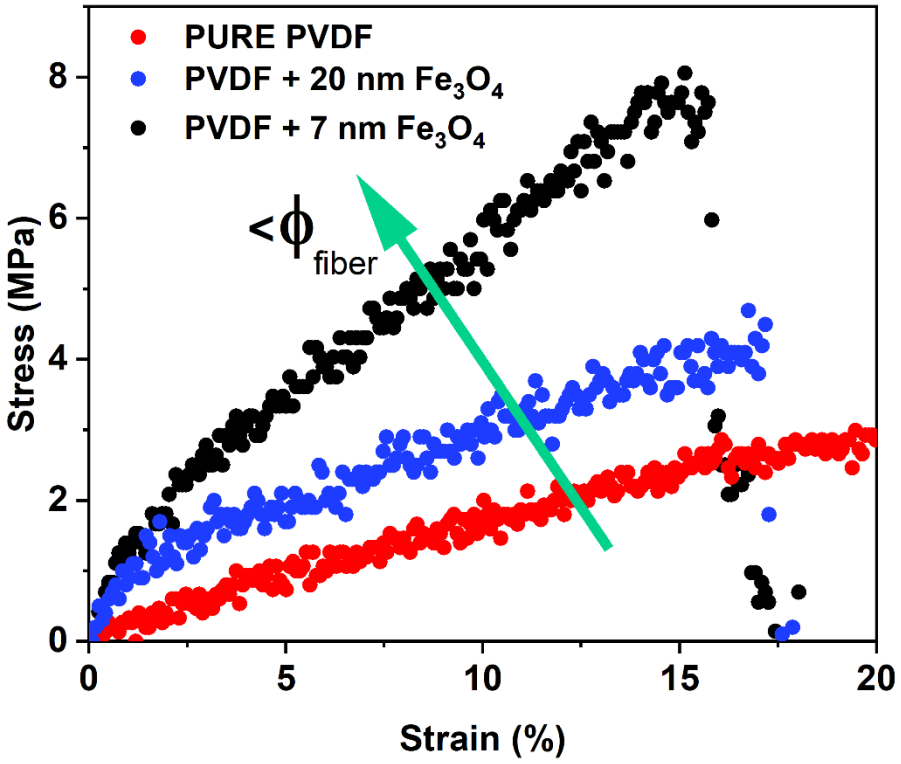

Figure 5 Stress–Strain curves of pure PVDF, PVDF - 20 nm Fe_3O_4 and PVDF - 7 nm Fe_3O_4 electrospun films

Altogether, this consideration justifies the higher performance of composites made of smaller NPs.

3.5 Structural characterization through XRD and MD simulation

It is well known that electrospinning is an efficient technique for producing PVDF nanofibers with a high β-phase content and crystallinity by aligning molecular dipoles along an applied voltage direction [4, 5]. α- and β-phases have different lattice parameters and symmetry and that translates into different XRD signatures. The XRD spectra of the α-phase show characteristic peaks at 2θ = 17.7°, 2θ = 18.4°, 2θ = 20° and 2θ = 26.6° corresponding to the (1 0 0), (0 2 0), (1 1 0 / 0 2 1) planes, and β-phase exhibits a peak at 2θ = 20.7° for the (1 1 0) and (2 0 0) planes [9, 40].

The content of the α- and β-phases of each electrospun film was determined by a peak deconvolution method [41]. The XRD spectra were decomposed into amorphous and crystalline regions using a curve fitting technique, as shown in **Figure 6**. The crystalline

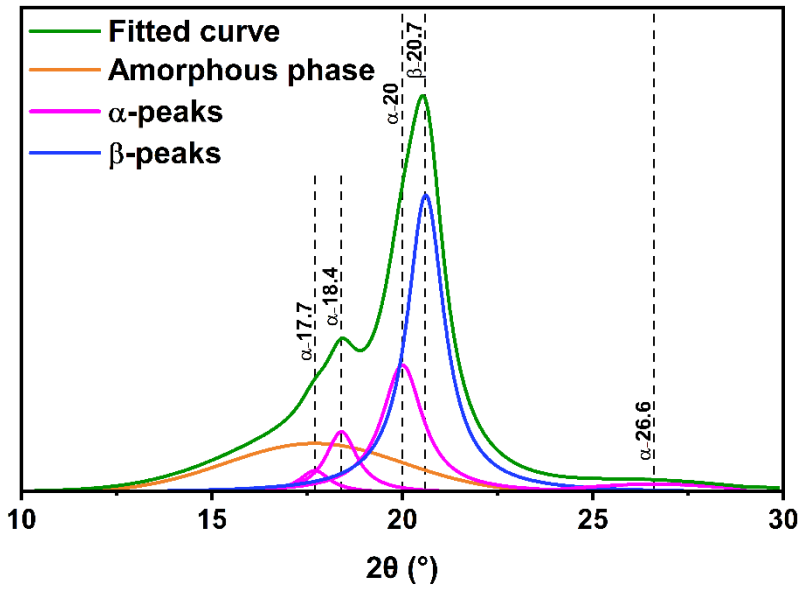

Figure 6 Deconvolution method and characteristic peaks of PVDF phases

peaks were fitted with Lorentzian functions and the amorphous halo with a Gaussian function [41]. The initial positions of crystalline peaks were set manually at known values and the amorphous halo was placed between 2θ =15° and 2θ =20°. After convergent iterations, the position of the amorphous halo was blocked, and the positions of the crystalline peaks were recalculated. The corresponding areas for the amorphous halo and crystalline peaks obtained were used to calculate the content of each PVDF phase. We defined the content of each phase as the area of its peaks divided by the total area under the fitted curve, as a percentage, as shown in equation (3) [41]:

$$(\alpha, \beta\%) = \frac{A_{\alpha,\beta}}{A_\alpha + A_\beta + A_{amorphous}} \times 100 \quad (3)$$

The results showed that the amount of β-phase for nanocomposites was lower when compared to the pure PVDF sample. Moreover, this amount decreased for smaller reinforcements, as shown in **Figure 7**.

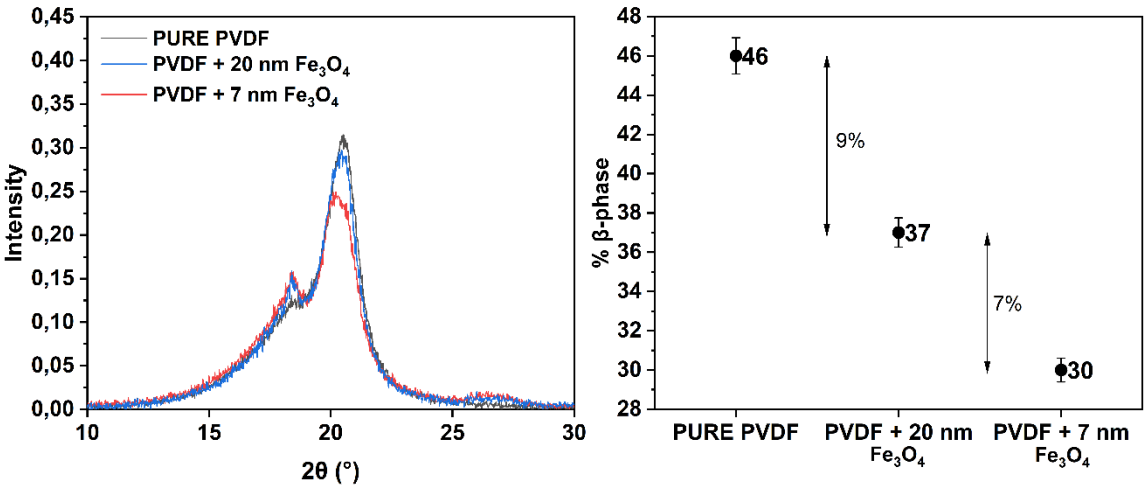

Figure 7 XRD patterns of electrospun pure PVDF, PVDF-Fe_3O_4 (20 nm) and PVDF-Fe_3O_4 (7 nm)

β-phase is generally obtained by stretching. These results seem to be in discordance with the fact that Fe_3O_4 nanoparticles are conductive and for equal volume fractions of nanoparticles, smaller nanoparticles induce higher stretching rates. Fiber size decreases as NP size decreases, which is what has led to this conclusion. For this reason, the decrease in the β-phase should be investigated further as we used commercially available NPs grafted with oleic acid. Oleic acid is used to stabilize NPs and helps to maintain their optimal dispersion in organic solvents [29, 42]. Polymer chains interact with NPs through the grafted oleic acid chains and possibly with oleic acid residues in the solution. It was not experimentally feasible to investigate interfacial interactions in our system. Therefore, two model systems made of Fe_3O_4 slabs with different surface chemistry in contact with α-PVDF chains were built to mimic, to some extent, our experimental case.

The two Fe_3O_4 surface configurations were OH- terminated Fe_3O_4 and oleic acid-grafted Fe_3O_4 as it is the configuration we encounter in commercially available NPs such as ours (**Figure 8**). OH- terminated Fe_3O_4 will be considered as a reference state that contrasts with

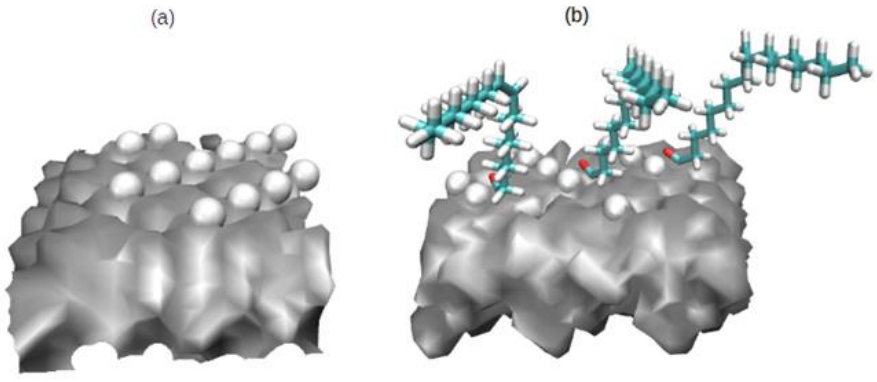

Figure 8 Cross sections of the magnetite slabs with (a) OH grafting and (b) 20% oleic acid grafting. The magnetite slab, OH groups and oleic acid modifications are shown using surface, vdW and CPK representations, respectively.

the previous option. Oleic acid is used to stabilize NPs and helps maintain their optimal dispersion in organic solvents [29, 42].

The average dipole moment (μ) of the α-PVDF layer was investigated on both configurations to understand the driving mechanism of α- to β-phase transition when PVDF chains interact with Fe_3O_4 surfaces. After the equilibration process described in a previous paper [6], NPT simulations were performed for 10 ns. During this simulation, the dipole moments of both systems were averaged. The values obtained were 72.03±8.19 and 42.39±5.95 debye for OH and 20% oleic acid modifications, respectively. **Figure 9** shows that replacing 20% of the OH groups with oleic acid causes a decrease of approximately 41% in the magnetite boostering effect on the electric properties of α-PVDF.

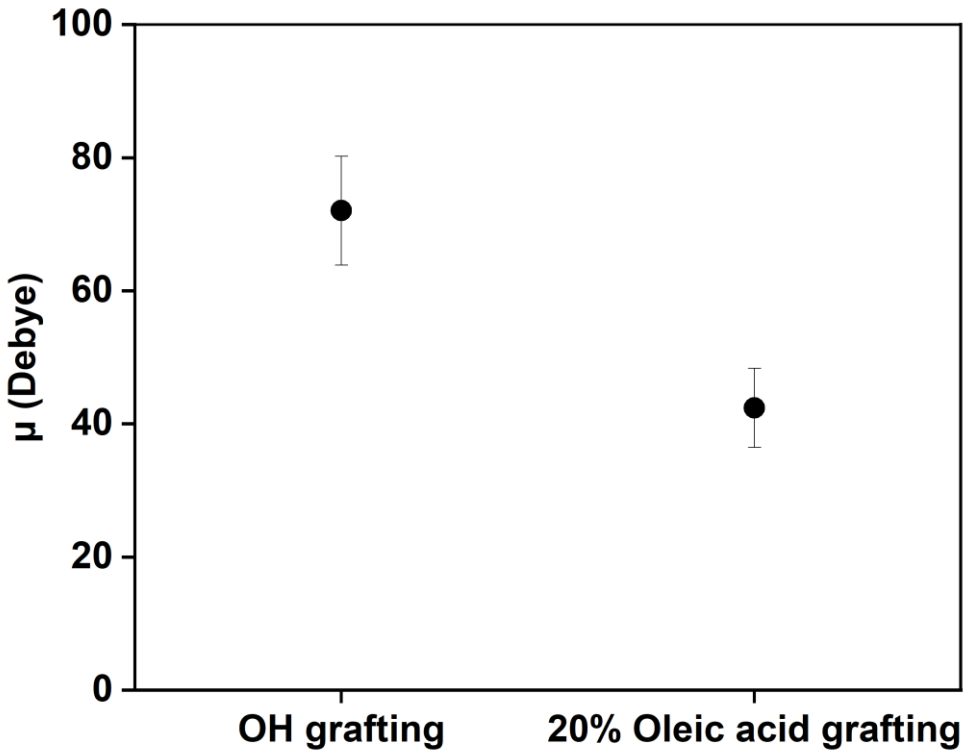

Figure 9 Average dipole moment for α-PVDF during 10 ns of MD simulation in the presence of magnetite with different surface treatments.

The results of the simulation showed that functionalizing the surface of the nanoparticles with oleic acid decreased the number of H-bond interactions between the chains of PVDF and the surface of the particle. The simulation considered that 20% of the OH groups were replaced with oleic acid. The nanoparticles used for this experience were functionalized with oleic acid. As the number of oleic acid molecules grafted to the surface of the nanoparticles is related to their surfaces, the nanocomposites with smaller nanoparticles have more oleic acid, and it is thus expected that they have lower β-phase percentages.

To validate these assumptions, we prepared two PVDF/oleic acid solutions with concentrations of 2% m/m and 4% m/m of oleic acid. These concentrations were chosen using an amount of oleic acid of 20% w/w in our nanoparticles, to emulate the quantity of oleic acid we have in our nanoparticle suspensions (2% m/m oleic acid - PVDF/oleic solution) and twice this quantity (4% m/m oleic acid - PVDF/oleic solution).

We prepared electrospun films with both solutions and determined their β-phase percentages through XRD (**Figure 10**).

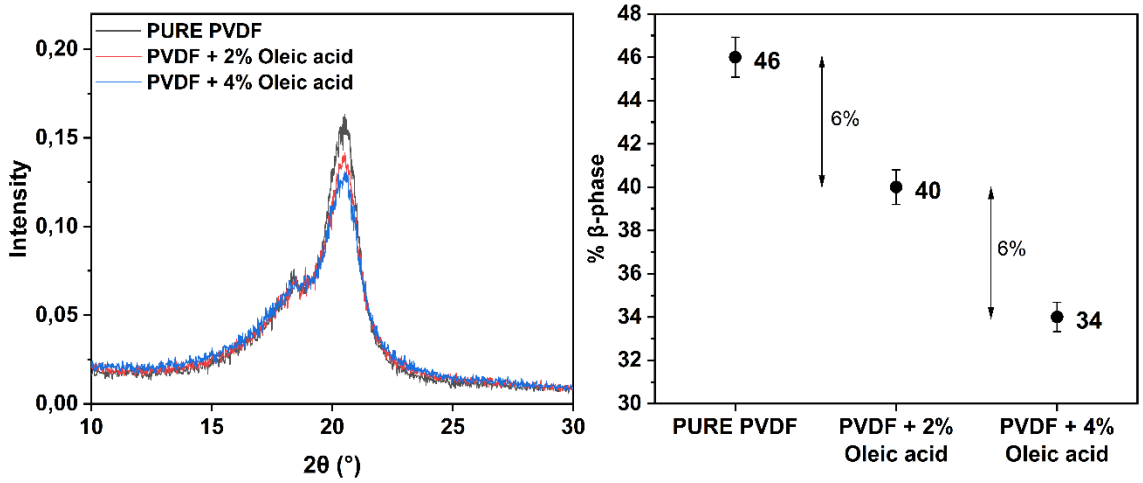

Figure 10 XRD patterns of electrospun pure PVDF, PVDF-oleic acid 2% w/w, and PVDF-oleic acid 4% w/w

The β-phase percentages determined from XRD patterns of PVDF with 2% w/w and 4% w/w of oleic acid are in accordance with the MD simulation approach and the results obtained experimentally for nanocomposites.

To confirm our MD simulation - experimental hypothesis regarding the possible effect of oleic acid, nanoparticles were washed with ethanol and toluene to eliminate the excess oleic acid at the surface [31]. We prepared electrospun films with washed nanoparticles and we observed that the β-phase percentages showed the same trend as unwashed NP electrospun films. However, 20 nm and 7 nm washed NP nanocomposites showed an increase of 7% and 12% respectively in the β-phase percentage. Thus, the difference in β-phase percentage referred to the pure PVDF sample decreased for both nanocomposites (**Figure 11**). The amount of oleic acid was reduced by washing with ethanol and toluene, but the molecules grafted remained attached to the surface, which explains this result.

The PVDF - Fe_3O_4 washed NP nanocomposites were annealed at 140 °C for 17 hours and then cooled down to room temperature. The XRD studies showed that the trend observed previously was inverted for PVDF - 7 nm Fe_3O_4 and PVDF – 20 nm Fe_3O_4 nanocomposites (**Figure 11**).

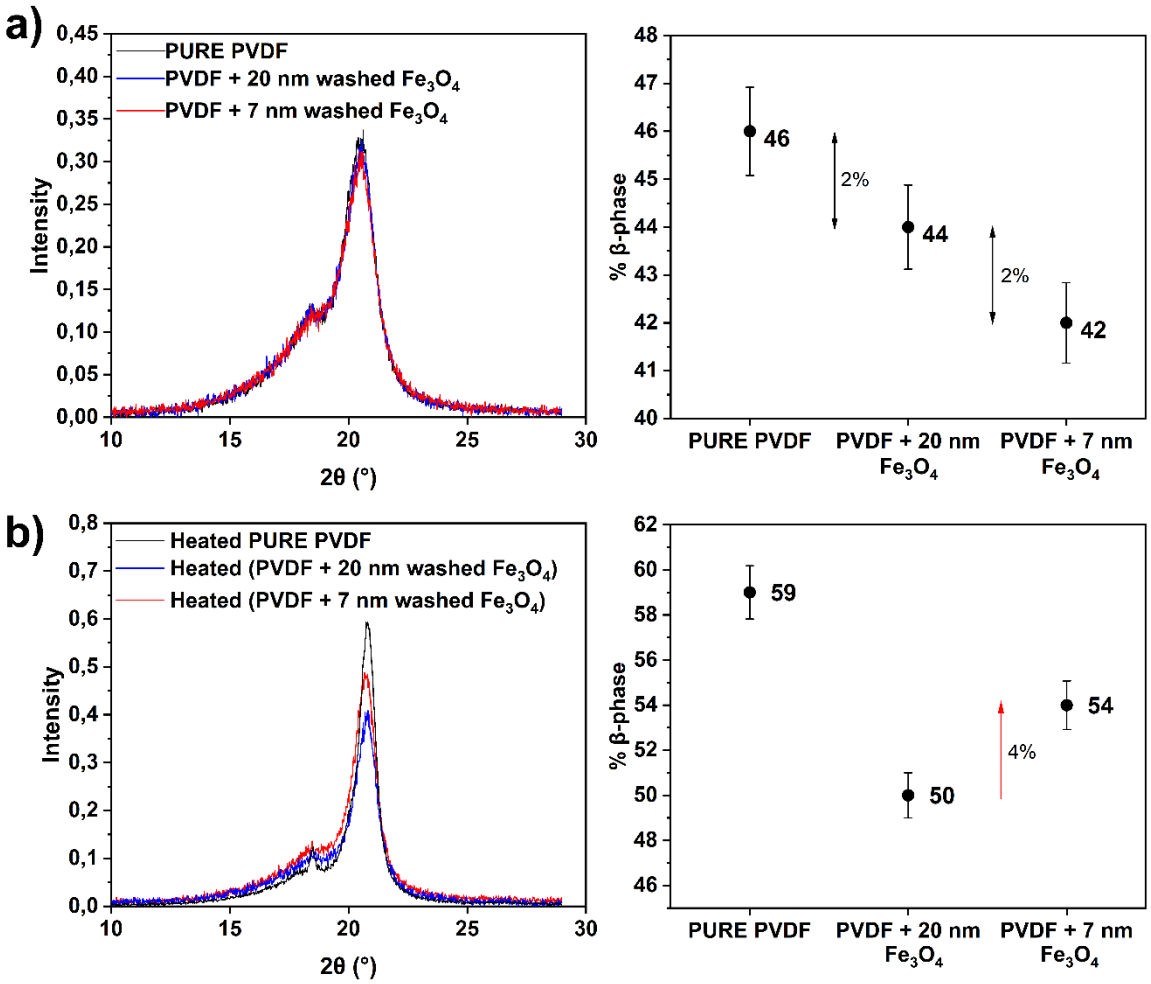

Figure 11 a) XRD patterns of electrospun pure PVDF, PVDF – 20 nm Fe3O4 (washed) and PVDF – 7 nm Fe3O4 (washed) – b) XRD patterns of electrospun pure PVDF, PVDF – 20 nm Fe_3O_4 (washed) and PVDF – 7 nm Fe_3O_4 (washed) after annealing treatment at 140°C for 17 hours

For pure PVDF, the α- to β-phase transition is favored at temperatures close to melting point (T_f = 160 °C). At 140°C, the chains of PVDF have more mobility and their interactions with the surface of the nanoparticles are boosted [14]. Moreover, cis-trans isomerization of oleic acid can occur when the temperature is greater than 120°C [43]. In our case, this reaction was

confirmed through FTIR spectroscopy by examining the characteristic peak at 966 cm^{-1} (**Figure 12aError! Reference source not found.**), corresponding to the C-H out-of-plane deformation vibration absorption band in trans fatty acids, such as elaidic acid [44]. As an unsaturated acid, oleic acid has the two parts of the carbon chain bent towards each other, while elaidic acid has an almost linear structure.

As suggested by the experimental results, straight ligands seem to not bend on the surface, leaving space for more efficient interaction between polymeric chain and the magnetite surface. To validate this assumption, we run simulation of PVDF layer and magnetite slab grafted with Elaidic acid. We used the same simulation procedure and used the same parameters. From this simulation, the dipole moment of the PVDF chains was computed. The use of Elaidic acid induces 25% increase compared to the Oleic acid which confirms our experimental data (**Figure 12b**).

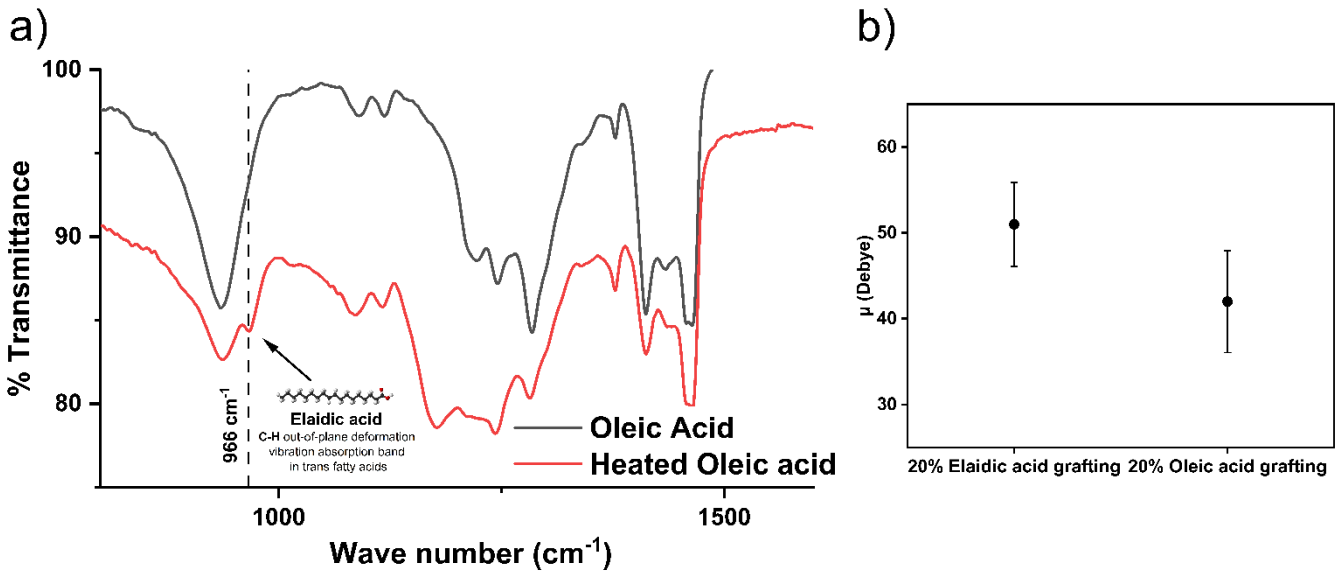

Figure 12 a) FTIR-ATR spectra of oleic acid before and after thermal treatment at 140 °C for 17 hours – b) Comparison of the dipole moment of PVDF chains and magnetic slabs with elaidic acid and oleic acid.

The linear configuration of elaidic acid releases more space that was previously occupied by oleic acid bent molecules (**Figure 13**). As such, PVDF chains can easily interact with the -OH termination of the nanoparticle as shown in the work by Sahihi et al. The high mobility of PVDF molecular chains allows the realignment of dipoles, and results in the transition from α-phase to β-phase. Nanocomposites with 7 nm NPs present higher interaction surfaces than their counterparts with 20 nm. This is due to the high surface-to-volume ratio in the case of smaller NPs. As such, composites with smaller NPs should undergo more transition from α-phase to β-phase. This case is bolstered by our experimental results.

It is worth noticing that the linearity of elaidic acid brings our systems closer to the case of NPs grafted with saturated acid molecules with shorter carbon chains, such as hexanoic acid, treated with MD simulation in a previous work [6]. In the following schematic model, we summarize our results through the different process steps we went through to prepare our samples.

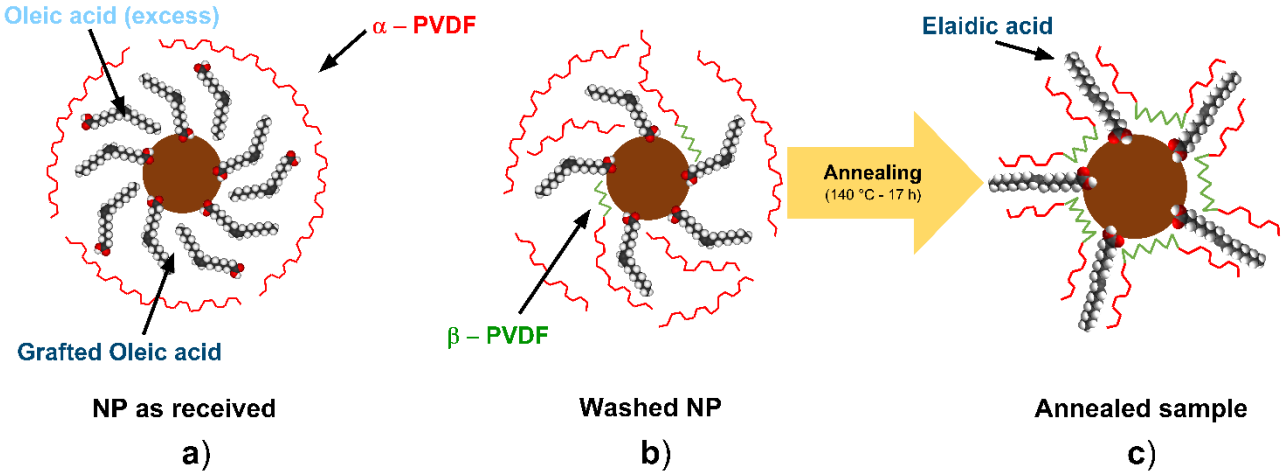

Figure 13 a) Surface interactions of PVDF chains with Fe_3O_4 nanoparticles (as received). **b)** Surface interactions of PVDF chains with Fe_3O_4 washed nanoparticles. **c)** Surface interactions of PVDF chains with Fe_3O_4 washed nanoparticles after annealing the samples.

4 CONCLUSIONS

We studied the morphology of electrospun fibers of PVDF, PVDF – 7 nm Fe_3O_4 and PVDF - 20 nm Fe_3O_4. For a constant volume fraction, smaller nanoreinforcements promoted thinner fibers. This result can be explained thanks to an increase in conductivity, a consequence of a higher number of conductive particles in the case of smaller reinforcements.

The fiber diameter determines the mechanical behavior of electrospun films. Thinner fibers undergo higher rates of entanglement and induce high molecule orientation resulting in stiffer materials.

At first, NP size appeared as an inhibitor for the β-phase polymorph. The presence of oleic acid chains on the surfaces prevents the α- to β-phase transition. This is related to the number of organic molecules grafted to the surface of the nanoparticles. As the surface-to-volume ratio increases for smaller nanoparticles, the number of molecules grafted increases as well. These results are in accordance with MD simulation results showing that the β-phase is less probable in the presence of oleic acid grafted on to Fe_3O_4 slabs.

By eliminating the excess oleic acid, the amount of β-phase in the nanocomposites globally increases and the difference in the amount of β-phase between the samples becomes smaller.

We found that the trend was reversed after annealing the films at 140°C for 17 hours. This phenomenon shows that when PVDF chains have the best conditions for molecular mobility, they organize into the beta configuration. Furthermore, oleic acid molecules undergo an isomerization reaction in this range of temperatures, producing elaidic acid, which is linear and releases more space for interactions between NPs and PVDF chains than oleic acid molecules. The surface of interaction between the PVDF chains and the nanoparticles is superior in the case of smaller nanoparticles and explains a greater increase in the amount of

β-phase in PVDF – 7 nm Fe_3O_4 after annealing. This trend inversion showed that the size effect of reinforcement is still a factor that promotes β-phase formation, when other conditions related to its surface chemistry are favorable.

We can derive from our results that the need to have oleic acid chains grafted on to the nanoparticle surface for stability and good dispersion purposes can impede the interaction of PVDF chains with the nanoparticle surface, diminishing the booster effect of the nano-fillers on the electric properties of PVDF nanocomposites. Tuning the grafted-chain conformation is another parameter that might enhance the macroscopic properties of nanocomposites.

Acknowledgement

This work was funded by the Région Hauts-de-France and the French Government, through the program "Investments for the future" managed by the National Agency for Research (reference ANR-11-IDEX- 0004-02) in the framework of the Labex MS2T.

References

[1] J.H. McFee, J.G. Bergman, G.R. Crane, Pyroelectric and nonlinear optical properties of poled polyvinylidene fluoride films, Ferroelectrics 3(1) (1972) 305-313.
[2] H. Kawai, The Piezoelectricity of Poly (vinylidene Fluoride), Japanese Journal of Applied Physics 8(7) (1969) 975-976.
[3] K.i. Nakamura, Y. Wada, Piezoelectricity, pyroelectricity, and the electrostriction constant of poly(vinylidene fluoride), Journal of Polymer Science Part A-2: Polymer Physics 9(1) (1971) 161-173.
[4] T. Lei, L. Yu, G. Zheng, L. Wang, D. Wu, D. Sun, Electrospinning-induced preferred dipole orientation in PVDF fibers, Journal of Materials Science 50(12) (2015) 4342-4347.
[5] Z. He, F. Rault, M. Lewandowski, E. Mohsenzadeh, F. Salaün, Electrospun PVDF Nanofibers for Piezoelectric Applications: A Review of the Influence of Electrospinning Parameters on the β Phase and Crystallinity Enhancement, Polymers (Basel) 13(2) (2021).
[6] M. Sahihi, A. Jaramillo-Botero, W.A. Goddard, F. Bedoui, Interfacial Interactions in a Model Composite Material: Insights into α → β Phase Transition of the Magnetite Reinforced Poly(Vinylidene Fluoride) Systems by All-Atom Molecular Dynamics Simulation, The Journal of Physical Chemistry C 125(39) (2021) 21635-21644.

[7] L. Ruan, X. Yao, Y. Chang, L. Zhou, G. Qin, X. Zhang, Properties and Applications of the β Phase Poly(vinylidene fluoride), Polymers 10(3) (2018).
[8] H.S. Nalwa, RECENT DEVELOPMENTS IN FERROELECTRIC POLYMERS, Journal of Macromolecular Science, Part C 31(4) (1991) 341-432.
[9] A.J. Lovinger, Poly(Vinylidene Fluoride), in: D.C. Bassett (Ed.), Developments in Crystalline Polymers—1, Springer Netherlands, Dordrecht, 1982, pp. 195-273.
[10] J.H. Kang, G. Sauti, C. Park, V.I. Yamakov, K.E. Wise, S.E. Lowther, C.C. Fay, S.A. Thibeault, R.G. Bryant, Multifunctional Electroactive Nanocomposites Based on Piezoelectric Boron Nitride Nanotubes, ACS Nano 9(12) (2015) 11942-50.
[11] T.S. Roopaa, H.N. Narasimha Murthy, V.V. Praveen Kumar, M. Krishna, Development and Characterization of PVDF Thin Films for pressure sensors, Materials Today: Proceedings 5(10, Part 1) (2018) 21082-21090.
[12] L. Jason, C.T. Pan, L.W. Lin, H.-W. Lai, Piezoelectric properties of PVDF/MWCNT nanofiber using near-field electrospinning, Sensors and Actuators A: Physical 193 (2013) 13–24.
[13] J. Defebvin, S. Barrau, G. Stoclet, C. Rochas, J.-M. Lefebvre, In situ SAXS/WAXS investigation of the structural evolution of poly(vinylidene fluoride) upon uniaxial stretching, Polymer 84 (2016) 148-157.
[14] Y. Zhu, H. Ye, L. Yang, L. Jiang, L. Zhen, J. Huang, Z. Jiao, J. Sun, Effect of Annealing Temperatures and Time on Structural Evolution and Dielectric Properties of PVDF Films, Polymers and Polymer Composites 24(2) (2016) 167-172.
[15] M. Satthiyaraju, T. Ramesh, Effect of annealing treatment on PVDF nanofibers for mechanical energy harvesting applications, Materials Research Express 6(10) (2019) 105366.
[16] H. Gade, S. Bokka, G.G. Chase, Polarization treatments of electrospun PVDF fiber mats, Polymer 212 (2021) 123152.
[17] V. Sencadas, R. Jr, S. Lanceros-Méndez, α to β Phase Transformation and Microestructural Changes of PVDF Films Induced by Uniaxial Stretch, Journal of Macromolecular Science® 48 (2009) 514-525.
[18] P.K. Szewczyk, A. Gradys, S.K. Kim, L. Persano, M. Marzec, A. Kryshtal, T. Busolo, A. Toncelli, D. Pisignano, A. Bernasik, S. Kar-Narayan, P. Sajkiewicz, U. Stachewicz, Enhanced Piezoelectricity of Electrospun Polyvinylidene Fluoride Fibers for Energy Harvesting, ACS Appl Mater Interfaces 12(11) (2020) 13575-13583.
[19] J.S. Andrew, J.J. Mack, D.R. Clarke, Electrospinning of polyvinylidene difluoride-based nanocomposite fibers, Journal of Materials Research 23(1) (2008) 105-114.
[20] J.Y. Lim, S. Kim, Y. Seo, Enhancement of β-phase in PVDF by electrospinning, AIP Conference Proceedings 1664(1) (2015) 070006.

[21] N. Chakhchaoui, R. Farhan, A. Eddiai, M. Meddad, O. Cherkaoui, M.h. Mazroui, Y. Boughaleb, L. Van Langenhove, Improvement of the electroactive β-phase nucleation and piezoelectric properties of PVDF-HFP thin films influenced by TiO2 nanoparticles, Materials Today: Proceedings 39 (2021) 1148-1152.
[22] S.A. Haddadi, S. Ghaderi, M. Amini, S.A.A. Ramazani, Mechanical and piezoelectric characterizations of electrospun PVDF-nanosilica fibrous scaffolds for biomedical applications, Materials Today: Proceedings 5(7, Part 3) (2018) 15710-15716.
[23] T. Lei, X. Cai, X. Wang, L. Yu, X. Hu, G. Zheng, W. Lv, W. Lingyun, D. Wu, D. Sun, L. Lin, Spectroscopic evidence for a high fraction of ferroelectric phase induced in electrospun polyvinylidene fluoride fibers, RSC Advances 3 (2013) 24952.
[24] H. Wang, Q. Fu, J. Luo, D. Zhao, L. Luo, W. Li, Three-phase Fe3O4/MWNT/PVDF nanocomposites with high dielectric constant for embedded capacitor, Applied Physics Letters 110(24) (2017) 242902.
[25] O. Jayakumar, E.H. Abdelhamid, V. Kotari, B.P. Mandal, R. Rao, V.M. Naik, R. Naik, A. Tyagi, Fabrication of flexible and self-standing inorganic–organic three phase magneto-dielectric PVDF based multiferroic nanocomposite films through a small loading of graphene oxide (GO) and Fe 3 O 4 nanoparticles, Dalton Transactions 44(36) (2015) 15872-15881.
[26] P. Martins, C. Caparros, R. Gonçalves, P.M. Martins, M. Benelmekki, G. Botelho, S. Lanceros-Mendez, Role of Nanoparticle Surface Charge on the Nucleation of the Electroactive β-Poly(vinylidene fluoride) Nanocomposites for Sensor and Actuator Applications, The Journal of Physical Chemistry C 116(29) (2012) 15790-15794.
[27] Y. Wu, S.L. Hsu, C. Honeker, D.J. Bravet, D.S. Williams, The Role of Surface Charge of Nucleation Agents on the Crystallization Behavior of Poly(vinylidene fluoride), The Journal of Physical Chemistry B 116(24) (2012) 7379-7388.
[28] L. Lenglet, L. Motte, Chapter 8 - Neel Effect: Exploiting the Nonlinear Behavior of Superparamagnetic Nanoparticles for Applications in Life Sciences up to Electrical Engineering, in: N. Domracheva, M. Caporali, E. Rentschler (Eds.), Novel Magnetic Nanostructures, Elsevier2018, pp. 247-265.
[29] L. Zhang, R. He, H.-C. Gu, Oleic acid coating on the monodisperse magnetite nanoparticles, Applied Surface Science 253(5) (2006) 2611-2617.
[30] H. Meng, Z. Zhang, F. Zhao, T. Qiu, J. Yang, Orthogonal optimization design for preparation of Fe3O4 nanoparticles via chemical coprecipitation, Applied Surface Science 280 (2013) 679-685.
[31] K. Yang, H. Peng, Y. Wen, N. Li, Re-examination of characteristic FTIR spectrum of secondary layer in bilayer oleic acid-coated Fe3O4 nanoparticles, Applied Surface Science 256(10) (2010) 3093-3097.
[32] M.J. Frisch, et al., , Gaussian 16 Rev. B.01, Wallingford, CT (2016).

[33] B. Hess, C. Kutzner, D. van der Spoel, E. Lindahl, GROMACS 4: Algorithms for Highly Efficient, Load-Balanced, and Scalable Molecular Simulation, Journal of Chemical Theory and Computation 4(3) (2008) 435-447.
[34] D. Van Der Spoel, E. Lindahl, B. Hess, G. Groenhof, A.E. Mark, H.J. Berendsen, GROMACS: fast, flexible, and free, J Comput Chem 26(16) (2005) 1701-18.
[35] F.S. Navarro Oliva, L. Picart, C.Y. Leon-Valdivieso, A. Benalla, L. Lenglet, A. Ospina, J. Jestin, F. Bedoui, Coaxial electrospinning process toward optimal nanoparticle dispersion in polymeric matrix, Polymer Composites 42(3) (2021) 1565-1573.
[36] A.S. Blivi, F. Benhui, J. Bai, D. Kondo, F. Bédoui, Experimental evidence of size effect in nano-reinforced polymers: Case of silica reinforced PMMA, Polymer Testing 56 (2016) 337-343.
[37] P. Chavoshnejad, O. Alsmairat, C. Ke, M.J. Razavi, Effect of interfiber bonding on the rupture of electrospun fibrous mats, Journal of Physics D: Applied Physics 54(2) (2020) 025302.
[38] X. Wei, Z. Xia, S.-C. Wong, A. Baji, Modelling of mechanical properties of electrospun nanofibre network, Int. J. Experimental and Computational Biomechanics Int. J. Experimental and Computational Biomechanics 1 (2009) 45-57.
[39] F. Bedoui, A. Jaramillo-Botero, T.A. Pascal, W.A. Goddard, Focus on the deformation mechanism at the interfacial layer in nano-reinforced polymers: A molecular dynamics study of silica - poly(methyl methacrylate) nano-composite, Mechanics of Materials 159 (2021) 103903.
[40] Y.-J. Kim, C.H. Ahn, M.B. Lee, M.-S. Choi, Characteristics of electrospun PVDF/SiO2 composite nanofiber membranes as polymer electrolyte, Materials Chemistry and Physics 127(1) (2011) 137-142.
[41] N.S. Murthy, H. Minor, General procedure for evaluating amorphous scattering and crystallinity from X-ray diffraction scans of semicrystalline polymers, Polymer 31(6) (1990) 996-1002.
[42] Y.-h. Zheng, Y. Cheng, F. Bao, Y.-s. Wang, Synthesis and magnetic properties of Fe3O4 nanoparticles, Materials Research Bulletin 41(3) (2006) 525-529.
[43] N. Cheng, J. Zhang, J. Yin, S. Li, Computational and experimental research on mechanism of cis/trans isomerization of oleic acid, Heliyon 4(9) (2018) e00768.
[44] E.B. Walker, D.R. Davies, M. Campbell, Quantitative Measurement of Trans-Fats by Infrared Spectroscopy, Journal of Chemical Education 84(7) (2007) 1162.